The Astrophysical Journal, 617:1353–1360, 2004 December 20

EXACT STEADY STATE RECONNECTION SOLUTIONS IN WEAKLY COLLISIONAL PLASMAS

P. G. Watson
Center for Magnetic Reconnection Studies, Institute for Fusion Studies, Department of Physics, University of Texas at Austin, 1 University Station C1500, Austin, TX 78712; pgwatson@kato.ph.utexas.edu

and

F. Porcelli
Burning Plasma Research Group, INFM and Department of Energetics, Politecnico di Torino, Corso Duca degli Abruzzi 24, 10129 Turin, Italy; porcelli@polito.it
Received 2004 March 26; accepted 2004 September 3

ABSTRACT

We consider the problem of reconnection in weakly collisional plasmas in the strong guide field limit. In this regime the standard resistive Ohm's law is modified to include electron compressibility and electron inertia effects. Despite the increased complexity of the governing equations, we show that analytic steady state solutions, like those discovered by Craig and Henton for the purely resistive case, can be developed for this new system. The resulting solutions are somewhat richer than those of Craig and Henton, and there are various different regimes in parameter space to consider that exhibit multiple length scales, boundary layer effects, and other features. We also examine the dynamical behavior of these new solutions by solving the time-dependent problem numerically.

Subject headings: MHD — plasmas

1. INTRODUCTION

Magnetic reconnection plays a fundamental role in the dynamics of all magnetized plasmas. Not only is it the mechanism that allows topological changes in magnetic structure, but it is also believed to be the process that underlies many of the explosive energy release events observed in both laboratory and astrophysical plasmas (Priest & Forbes 2000; Vasyliunas 1975; Biskamp 2000). Although the bulk of early reconnection research involved the study of collisional plasmas, more recently the focus has shifted to examining weakly collisional or collisionless plasmas where the effects of other nonideal terms are included in the generalized Ohm's law (Schep et al. 1994; Bhattacharjee et al. 1999; Birn et al. 2001; Shay et al. 2001).

One interesting advance in recent years was the discovery by Craig & Henton (1995) of an exact reconnection solution for resistive single-fluid plasmas. This simple two-dimensional solution has since been modified to include the effects of three-dimensionality, time dependence, and different spatial geometries (Craig & Fabling 1996, 1998; Watson & Craig 2002). In this paper we extend the Craig & Henton solution to the two-fluid framework more appropriate for collisionless or semicollisional plasmas. In particular, we explore the limit of a relatively strong guide field, for which the governing equations for the plasmas dynamics reduce to a simplified two-dimensional model. This approach augments other work by Craig & Watson (2003) and Craig et al. (2003) on the Hall MHD limit.

As in Craig & Henton (1995), we observe that "fast" reconnection solutions, for which the electric field E at the X-point scales independently of the resistivity, can in principle always be constructed by a suitable choice of external boundary conditions. However, severe pressure constraints on the solution effectively limit the range of parameter space for which such fast solutions are valid (see Craig & Henton 1995; Craig & Watson 2000). In addition, in accordance with Craig & Henton (1995), we only find steady state solutions in the limit of super-Alfvénic inflow.

This paper is organized as follows. In § 2 we describe the model, stating the underlying assumptions and sketching a derivation of the simplified two-dimensional system. In § 3 we derive new steady state solutions of this system and provide a description of their properties. In § 4, the dynamical behavior of these new solutions is examined by solving the time-dependent problem numerically. In doing so, the wavelike nature of the dynamical process is emphasized. Our conclusions are presented in § 5.

2. MODEL EQUATIONS

The model on which our analysis is based is the small ion Larmor radius limit of the model derived by Schep et al. (1994) and extensively investigated by Grasso et al. (2001) (see also Porcelli et al. 2002). Our model also agrees with the well-known four-field model presented in Hazeltine et al. (1985), neglecting the ion Larmor radius effects and the ion dynamics along magnetic field lines while retaining the electron compressibility effects in the generalized Ohm's law. These models apply to a low-β plasma ($\beta =$ kinetic pressure/magnetic pressure) in the presence of a guide field, more precisely, when $\beta = 8\pi p/B_0^2 < 1$, where B_0 is the guide-field component. Another important assumption is that the ion skin depth, $d_i = c/\omega_{pi}$ is smaller than the magnetic shear length, $l_0 = B_0/B'_\perp$, which again involves the guide field ($l_0 = 0$ if $B_0 = 0$); when $d_i \geq l_0$, Hall physics effects associated with the ion skin depth scale become important. Here $B'_\perp$ is a characteristic value of the modulo of the gradient of the magnetic field component on the x-y plane. The models assume two-dimensional dynamics, with one ignorable spatial coordinate, which we take to be along the z-direction.

The derivation of our model is briefly sketched in the following. We begin by describing a fully ionized hydrogen plasma as a quasi-neutral two-fluid system composed of electrons and ions. For the sake of simplicity we close the fluid system by assuming cold ions, isotropic stress tensors, and constant electron temperature.

The electron and ion momentum equations can be added to give a momentum balance equation

$$\sum_{\alpha=e,i} nm_\alpha \frac{D^\alpha \boldsymbol{u}_\alpha}{Dt} = \boldsymbol{J}\times\boldsymbol{B} - \nabla p_e, \quad (1)$$

where the index α labels the electron and ion species, n is the number density of both electrons and ions (quasi neutrality), m_α are the particle masses, $D^\alpha/Dt = \partial/\partial t + \boldsymbol{u}_\alpha\cdot\nabla$ is the convective derivative, $\boldsymbol{u}_\alpha$ are the velocities, $\boldsymbol{B}$ is the magnetic field, $\boldsymbol{J} = \nabla\times\boldsymbol{B} = ne(\boldsymbol{u}_i - \boldsymbol{u}_e)$ is the current density, $p_e = nT_e$ is the electron pressure, T_e is the constant electron temperature, and $p_i = 0$.

The electron momentum equation can be rewritten in the form of a generalized Ohm's law

$$\boldsymbol{E} + \boldsymbol{u}_i \times \boldsymbol{B} = \eta\boldsymbol{J} + \frac{1}{ne}(\boldsymbol{J}\times\boldsymbol{B} - \nabla p_e) - \frac{m_e}{e}\frac{D^e\boldsymbol{u}_e}{Dt}, \quad (2)$$

where $\boldsymbol{E}$ is the electric field, e is the charge of the electron, and η is the collisional resistivity (assumed constant). The terms on the right side of equation (2) are the resistive, Hall, electron pressure, and electron inertia terms, respectively.

In the strong guide field limit the ion flow is incompressible, and so the ion flow and the magnetic field can be represented as follows:

$$\begin{aligned}\boldsymbol{u}_i(x,y,t) &= \hat{\mathbf{z}}\times\nabla\phi(x,y,t) + v_z(x,y,t)\hat{\mathbf{z}},\\ \boldsymbol{B}(x,y,t) &= \nabla\psi(x,y,t)\times\hat{\mathbf{z}} + B_z(x,y,t)\hat{\mathbf{z}},\end{aligned} \quad (3)$$

where $B_z = B_0 + b_z$ and B_0 is the constant field guide.

Under the assumptions listed in the first paragraph of this section, we find that the equation for the perpendicular velocity v_z decouples from the rest of the system, while the equation for b_z mimics the vorticity equation, leading us to identify $b_z = \rho_s U$. Equations (1) and (2) can then be reduced to the following simplified set:

$$U_t + [\phi, U] = [J, \psi], \quad (4)$$

$$(\psi + d_e^2 J)_t + [\phi, \psi + d_e^2 J] = \rho_s^2[U,\psi] + \eta\nabla^2\psi, \quad (5)$$

where $U = \nabla^2\phi$ is the vorticity, $J = -\nabla^2\psi$ is the current density, $[f,g] = \boldsymbol{e}_z\cdot\nabla f\times\nabla g$, and subscripts on the basic variables ϕ, ψ, U, and J refer to partial differentiation; $d_e = c/\omega_{pe}$ is the electron inertial skin depth, $\rho_s = v_s/\Omega_0$ is the sonic Larmor radius with $v_s = \sqrt{T_e/m_i}$, and $\Omega_0 = eB_0/m_i c$ is the ion cyclotron frequency based on the guide field. All quantities appearing in equations (4) and (5) are dimensionless; a macroscopic length scale, $L = 1$, and the characteristic Alfvén time, $\tau_A = \sqrt{4\pi m_i n}/B'_\perp$, have been used in the normalization. The parameter η is the inverse of the magnetic Lundquist number.

Two comments are in order. First, the scale length d_i does not enter equations (4) and (5), consistent with the ordering $d_i < l_0$; indeed, equations (4) and (5) can be obtained from the generalized Ohm's law, equation (2), where the $\boldsymbol{J}\times\boldsymbol{B}$ Hall term is set to zero from the start. Second, the ion flow component along the ignorable direction, v_z, does not enter equations (4) and (5), consistent with the low-β ordering; this can also be seen from the four-field model of Hazeltine et al. (1985), where for small β the parallel ion flow decouples from the other variables, allowing a reduction from four equations to the two coupled equations (4) and (5).

3. EXACT STEADY STATE SOLUTIONS

We are interested in finding steady state solutions of equations (4) and (5) with $\psi_t = -E$, where E is a constant electric field in the z-direction (constant in both space and time). Following Craig & Henton (1995) we write ϕ and ψ in the form

$$\phi = M_A xy + f(x), \quad (6)$$

$$\psi = xy + g(x) - Et \quad (7)$$

[i.e., $\boldsymbol{u}_i = (-M_A x, M_A y + f', 0)$ and $\boldsymbol{B} = (x, -y - g', 0)$]. Following the normalization indicated in § 2, it is clear that the part of the magnetic flux function that pertains to hyperbolic field lines (i.e., setting $g = 0$) in dimensional units corresponds to $\psi = B'_\perp xy$, while the parameter M_A is the Alfvénic Mach number, corresponding to the hyperbolic part of the flow pattern relative to the hyperbolic part of the magnetic flux function. Also, the electric field is written in units of $c\tau_A B'_\perp$.

Substituting these forms into the steady version of equation (4) we find

$$f = \frac{1}{M_A}g + q, \quad (8)$$

where q is an arbitrary quadratic in x. In what follows we set $q = 0$, as it has very little impact on the reconnection physics.

From the steady state version of equation (5) we find

$$AxG'' + \eta G' + CxG = E, \quad (9)$$

where $G = -g'$ is the shear term in the B_y component of the magnetic field,

$$A = \frac{\rho_s^2}{M_A}(1-r), \quad C = \frac{M_A^2 - 1}{M_A}, \quad (10)$$

and

$$r = \frac{d_e^2 M_A^2}{\rho_s^2} = \frac{2m_e}{m_i}\frac{M_A^2}{\beta}. \quad (11)$$

The solutions of interest are such that $G(x)$ is a localized, odd function of x; thus, we require as boundary conditions

$$G(0) = 0, \quad G(x\to\infty) = 0. \quad (12)$$

We observe that an even part of $G(x)$ would not contribute to the reconnection process; however, it can be easily added if one so desires, since the general solution of equation (9) can be easily found analytically, as it is shown in the following. In addition, one may want to consider the problem on a finite integration domain, extending up to a maximum distance $x = \pm x_{max}$; in this case, the solutions of interest decay away with increasing $|x|$, i.e., $G(x)$ has a negative slope at $x = \pm x_{max}$, although a nonzero value of $G(x = x_{max})$ can be allowed.

Analysis of equation (9) indicates that only positive values of the coefficient C lead to well-behaved solutions satisfying the boundary conditions (12), as shown below. This was also true in the original work by Craig & Henton (1995), in which only super-Alfvénic flows allowed for well-behaved, stationary solutions.

Thus, there are three cases to consider, depending on the sign of the coefficient A. The first case, $A = 0$, corresponds to the case treated by Craig & Henton; thus, we review it first.

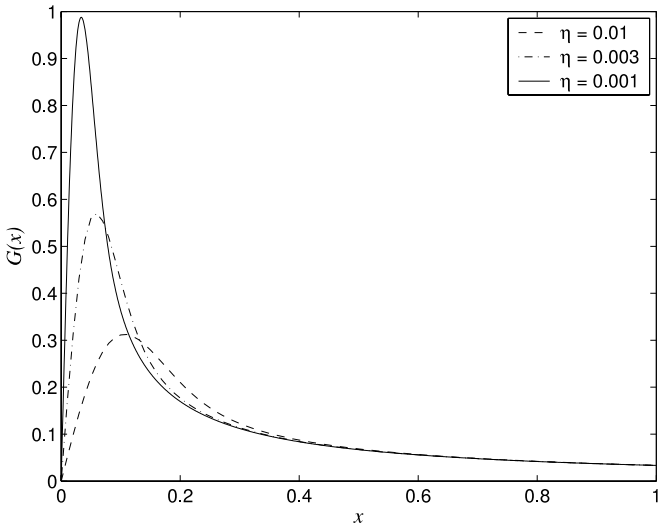

FIG. 1a

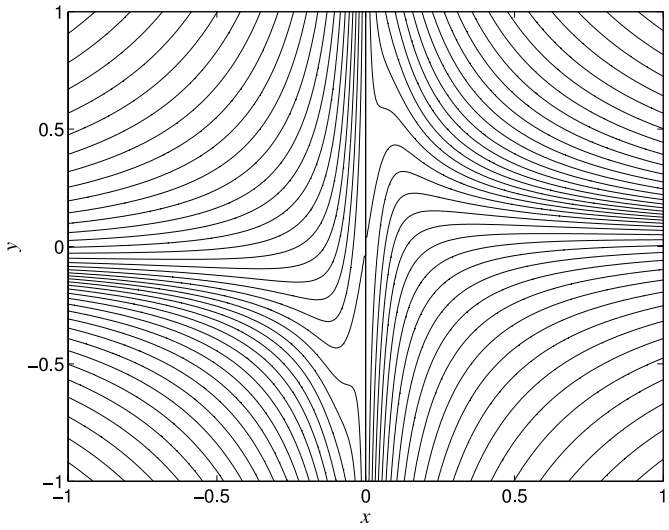

FIG. 1b

FIG. 1.—(*a*) Plots of the Dawson function magnetic shear component $G(x)$ versus x when $A = 0$ for various values of η and for $E = 0.05$ and $M_A = 2$. Note how the solutions localize and grow in amplitude as η is decreased. (*b*) Total field lines for the $A = 0$ (Craig & Henton 1995) solution with $\eta = 0.003$. Flux enters through the wide lobes, reconnects, and is ejected out of the narrow lobes of the X-point. The flux surfaces have been irregularly spaced to highlight the field structure near the separatrices.

Case 1: $A = 0$.—The purely resistive case with $A = 0$ was discussed in detail in Craig & Henton (1995); thus, we only give a brief summary here. Equation (9) reduces to

$$G' + 2\sigma^2 xG = E/\eta, \tag{13}$$

where $\sigma^2 = (M_A^2 - 1)/(2M_A\eta)$. Note that although Craig & Henton derived equation (13) from a model where $\rho_s = d_e = 0$, this equation is also valid for the special case $r = 1$.

The solution of equation (13) that satisfies the boundary conditions (12) is

$$G(x) = \frac{E}{\eta\sigma}\,\mathrm{daw}(\sigma x), \tag{14}$$

where daw(z) is the Dawson function given by

$$\mathrm{daw}(z) = e^{-z^2}\int_0^z e^{t^2}\,dt,$$

while the current density $\boldsymbol{J} = J\hat{\boldsymbol{z}}$ is given by

$$J(x) = G'(x) = \frac{E}{\eta}\left[1 - 2\sigma x\,\mathrm{daw}(\sigma x)\right]. \tag{15}$$

The important features of this solution are that it contains a single small length scale $1/\sigma$ and that the amplitude of the magnetic field scales as $E/(\eta\sigma)$. If E and M_A are fixed by an appropriate choice of boundary conditions and η is allowed to vary, then this solution implies that the length scale is given by $\eta^{1/2}$, while the magnitude of the field and current in the sheet scale as $B_s \sim \eta^{-1/2}$ and $J_s \sim \eta^{-1}$, respectively.

At first glance these scalings would seem to imply that fast reconnection (where the reconnection rate scales independently of the plasma resistivity) can always be achieved. This naive assumption can quickly be dispelled if one tries to recover the gas pressure from the momentum equation. What one finds is that the background gas pressure necessary to sustain such solutions scales as $p_0 \sim \eta^{-1}$. This implies that the fast solutions (with fixed inflow conditions) must become unphysical at some point. This problem was pointed out in Craig & Henton (1995), and its implications have been discussed in detail in Craig & Watson (1999, 2000).

Figure 1*a* shows profiles of the shear magnetic field component $G(x)$ for fixed inflow conditions and various values of η. Note the decrease of the length scale associated with the solution and the increase in its amplitude as η is decreased. It is the growth in field amplitude, or flux pileup, as η is reduced that leads to the pressure problem.

Figure 1*b* shows magnetic field lines (contours of ψ) for the $\eta = 0.003$ case shown in Figure 1*a*. These types of reconnection solutions have highly sheared magnetic X-points. Field lines enter the reconnecting current sheet, aligned along the y-axis, through the two wide lobes and are ejected, via a magnetic slingshot effect, out of the two narrow lobes.

Case 2: $A > 0$.—Let us consider now the case where $\rho_s > M_A d_e$ and the coefficient A is positive. The limiting case in which $d_e \to 0$ and ρ_s is finite is included in this discussion. Let us introduce the definitions

$$\gamma = \eta/A, \qquad \delta^2 = A/C, \qquad \mathcal{E} = E\delta/A \tag{16}$$

and the normalized distance

$$z = x/\delta. \tag{17}$$

Thus, equation (9) becomes

$$z^2G'' + \gamma zG' + z^2G = \mathcal{E}z. \tag{18}$$

This equation has the general solution

$$G(z) = z^{-\nu}[c_1J_\nu(z) + c_2Y_\nu(z)] + \mathcal{E}\sqrt{\pi}2^{\nu-1}\Gamma\left(\nu + \tfrac{1}{2}\right)z^{-\nu}\boldsymbol{H}_\nu(z), \tag{19}$$

where $\nu = (\gamma - 1)/2$ and $\boldsymbol{H}_\nu(z)$ is a Struve function (see Abramowitz & Stegun 1972, p. 495). The boundary condition

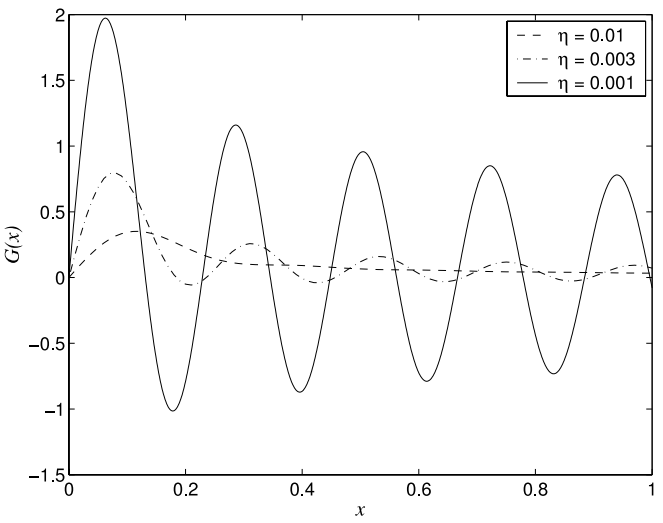

FIG. 2*a*

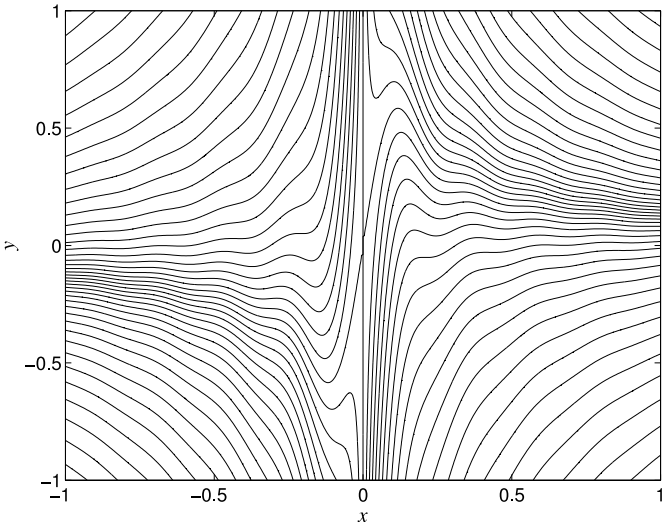

FIG. 2*b*

FIG. 2.—(*a*) Plots of the Struve function magnetic shear component $G(x)$ versus x when $A > 0$ for various values of η and for $E = 0.05$, $M_A = 2$, $\rho_s = 0.1$, and $d_e = 0.04$. These solutions develop oscillations as η is decreased. Also note that the growth in amplitude of the solutions as η is decreased is more severe than for the collisional Dawson function solutions. (*b*) Total field lines for the $A > 0$ solution with $\eta = 0.003$. The oscillations in the shear field component G appear as wavy structures in the total magnetic field.

$G(0) = 0$ implies both c_1 and c_2 are zero; this follows because $z^{-\nu}J_\nu(z)$ is an even function of z (for all ν) and $z^{-\nu}Y_\nu(z)$ is singular (or has a singular first derivative) at $z = 0$.

Hence, the relevant solution is

$$G(z) = \mathcal{E}\sqrt{\pi}2^{\nu-1}\Gamma\left(\nu + \tfrac{1}{2}\right)z^{-\nu}\boldsymbol{H}_\nu(z), \tag{20}$$

with current density

$$J = \frac{1}{\delta}\frac{dG}{dz} = \frac{\mathcal{E}}{2\delta}\left[\frac{1 - 2^\nu\sqrt{\pi}\Gamma(\nu + 3/2)z^{-\nu}\boldsymbol{H}_{\nu+1}(z)}{\nu + 1/2}\right]. \tag{21}$$

This solution has a number of interesting properties. In the collisional limit, obtained by assuming $\gamma, \nu \to \infty$ and $\delta \to 0$, we recover the Dawson function solution of Case 1. As ν is decreased, the solution begins to develop oscillations and also grows in amplitude. As we approach the collisionless limit $\eta = \gamma = 0$ and $\nu = -1/2$, the solution tends to an unbounded sinusoidal oscillation as

$$\lim_{\nu=-1/2} z^{-\nu}\boldsymbol{H}_\nu(z) = \sqrt{\frac{2}{\pi}}\sin z, \qquad \lim_{\nu=-1/2}\Gamma(\nu + \tfrac{1}{2}) = \infty.$$

The solution also undergoes a transition in typical length scale from the resistive length scale $l_r = 1/\sigma$ to the collisionless length scale $l_c = \delta$ as the parameter ν is reduced. Hence the quantity γ, which can also be expressed as $\gamma = l_r^2/l_c^2$, effectively measures the ratio of the competing length scales. The oscillations that develop are on the collisionless length scale and are presumably standing waves.

Figure 2*a* shows plots of the Struve function solution for fixed values of ρ_s and d_e and various values of η. The most obvious difference between these solutions and the collisional solutions is the development of large-scale oscillations in the outer field. A less obvious feature, but one that has an important consequence that we will discuss later, is the increase in amplitude of the solution when compared to the similar solution in the $A = 0$ limit (note the different scales on the axes for the two cases). In essence, the flux pileup associated with the Struve function solutions is more severe than that for the collisional Dawson function solutions.

Another interesting feature of the Struve function solution is that for half-integer powers of ν, we can express the solution in terms of elementary trigonometric and polynomial functions. For example, the first few solutions for $\nu = 1/2,\ 3/2$ are

$$G(z) = \frac{\mathcal{E}(1 - \cos z)}{z} \qquad \text{for } \nu = \tfrac{1}{2},$$
$$G(z) = \frac{\mathcal{E}(2 + z^2 - 2\cos z - 2z\sin z)}{z^3} \qquad \text{for } \nu = \tfrac{3}{2}. \tag{22}$$

There is one final point to make about the collisionless limit. If we return to equation (18) and let $\eta = \gamma = 0$, then we can solve the equation directly to obtain the solution

$$G(z) = c_1\sin z + c_2\cos z + \mathcal{E}[\sin z\,\mathrm{Ci}(z) - \cos z\,\mathrm{Si}(z)], \tag{23}$$

where $\mathrm{Ci}(z)$ and $\mathrm{Si}(z)$ are the cosine and sine integral functions, respectively, as defined in Abramowitz & Stegun (1972). The limit of the Struve function solution as $\eta \to 0$ is *not* the last term on the right of equation (23). The limit is in fact $G = c_1\sin z$, where $c_1 \to \infty$.

Case 3: $A < 0$.—When $\rho_s < M_A d_e$, so that the coefficient A is negative, we introduce the definitions

$$\bar{\gamma} = \eta/|A|, \qquad \bar{\delta}^2 = |A|/C, \qquad \bar{\mathcal{E}} = E\bar{\delta}/|A| \tag{24}$$

and the new normalized distance $z = x/\bar{\delta}$. Thus, equation (9) becomes

$$-z^2G'' + \bar{\gamma}zG' + z^2G = \bar{\mathcal{E}}z. \tag{25}$$

Note that the limiting case in which $\rho_s \to 0$ and d_e is finite is covered by this discussion.

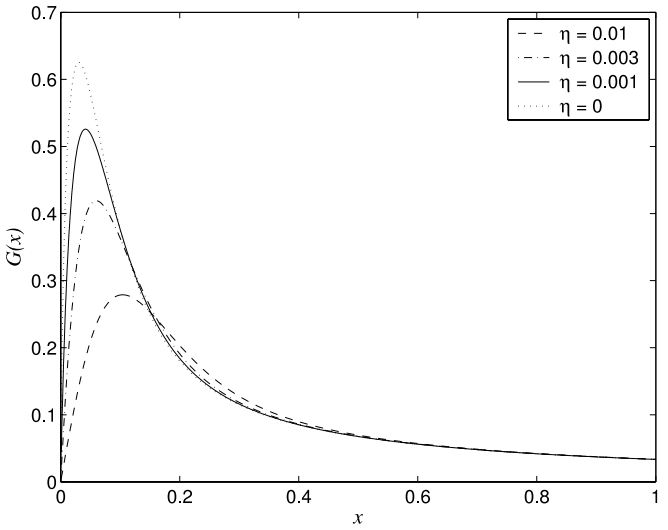

FIG. 3.—Plots of solution (26) for the magnetic shear component $G(x)$ versus x when $A < 0$ for various values of η and for $E = 0.05$, $M_A = 2$, $\rho_s = 0.08$, and $d_e = 0.05$. These solutions resemble the collisional solutions in Fig. 1; however, the increase in amplitude as η is decreased is less dramatic and is in fact bounded as $\eta \to 0$.

The solution of equation (25) that satisfies the boundary conditions (12) is

$$G(z) = \bar{\mathcal{E}} z^{\mu} \left[K_{\mu}(z) \int_0^z \frac{I_{\mu}(s)}{s^{\mu}}\, ds + I_{\mu}(z) \int_z^{\infty} \frac{K_{\mu}(s)}{s^{\mu}}\, ds \right], \qquad (26)$$

where $\mu = (\bar{\gamma} + 1)/2$ and the current associated with this solution is given by

$$J = \frac{\bar{\mathcal{E}} z^{\mu}}{\bar{\delta}} \left[- K_{\mu-1}(z) \int_0^z \frac{I_{\mu}(s)}{s^{\mu}}\, ds + I_{\mu-1}(z) \int_z^{\infty} \frac{K_{\mu}(s)}{s^{\mu}}\, ds \right]. \qquad (27)$$

For this solution the collisional limit is obtained by letting $\mu, \bar{\gamma} \to \infty$ and $\bar{\delta} \to 0$. If we fix $\bar{\delta}$ and reduce μ (equivalent to making the problem more and more collisionless), we find that the solutions localize and grow, but, in contrast to the $A > 0$ case, no oscillations develop. The solutions are more reminiscent of the $A = 0$ case; however, the amplitude of the solutions is now bounded as $\eta \to 0$. This behavior is shown in Figure 3, which shows plots of the $A < 0$ solutions for fixed values of ρ_s and d_e and various values of η.

The integrals in equation (26) can be solved in terms of elementary functions when μ assumes half-integer values. For example,

$$G(z) = \frac{\bar{\mathcal{E}}}{2} \Big[(\cosh z - z \sinh z)\mathrm{Shi}(z) - (\sinh z - z \cosh z)\mathrm{Chi}(z) \Big] \qquad \text{for } \mu = \tfrac{3}{2},$$

$$G(z) = \frac{\bar{\mathcal{E}}}{8} \Big[(3\cosh z - 3z \sinh z + z^2 \cosh z)\mathrm{Shi}(z) - (3\sinh z - 3z \cosh z + z^2 \sinh z)\mathrm{Chi}(z) - z \Big] \quad \text{for } \mu = \tfrac{5}{2},$$

where $\mathrm{Chi}(z)$ and $\mathrm{Shi}(z)$ are the hyperbolic cosine and sine integrals as defined in Abramowitz & Stegun (1972). Indeed we can even write the solution for the collisionless limit ($\eta = \bar{\gamma} = 0$, $\bar{\mu} = 1/2$)

$$G(z) = c_1 \sinh z + c_2 \cosh z + \bar{\mathcal{E}} [\cosh z \mathrm{Shi}(z) - \sinh z \mathrm{Chi}(z)]. \qquad (28)$$

Now the particular solution (proportional to $\bar{\mathcal{E}}$) *is* the limiting form of solution (26) as $\eta, \bar{\gamma} \to 0$, i.e., the coefficients c_1 and c_2 can be set to zero in equation (28).

The bounded $\eta = 0$ solution is shown in Figure 3 as the dotted line. The fact that the solution is bounded in the collisionless limit means that it avoids the pressure problem associated with the flux pileup exhibited in the $A = 0$ and $A > 0$ cases. The contour lines of ψ look qualitatively similar to those of Figure 1*b* (obtained for $A = 0$); therefore, we do not repeat them here.

It is important to note that the solution we have derived for the $A < 0$ case has badly behaved higher derivatives at the origin. To see this, let us consider the standard Frobenius series solution of equation (25) valid for small z. We find, for $\bar{\gamma}$ not equal to an integer, that

$$G(z) \sim \frac{\bar{\mathcal{E}}}{\bar{\gamma}} \left[z - \frac{z^3}{3(\bar{\gamma} - 2)} + \ldots \right] + d_1 z^{\bar{\gamma}+1} \left[1 + \frac{z^2}{2(\bar{\gamma} + 3)} + \ldots \right], \qquad (29)$$

where we have ignored terms that are nonzero at $z = 0$. The constant d_1 is fixed by setting the boundary condition at infinity and, in general, cannot be set to zero. This solution implies that although both G and G' are well behaved at $z = 0$, the higher derivatives will eventually become singular no matter how large we make $\bar{\gamma}$. When $\bar{\gamma}$ is an integer, the series expansion contains logarithmic terms, which are also singular at the origin.

Although singular derivatives are acceptable from a mathematical standpoint, the same is not strictly true physically or even numerically. In the physical problem, or when we attempt to solve the problem numerically, we must call on a higher-order dissipative process such as hyperresisitivity (or electron viscosity) in order to smooth out these singularities. It turns out that, numerically, this is only a problem if $\bar{\gamma} < 1$, when the second derivative becomes singular.

4. TIME-DEPENDENT SOLUTIONS

An interesting question is whether the steady solutions of § 3 are stable. Unfortunately, determining the stability of these solutions to fully two-dimensional or three-dimensional perturbations is beyond the scope of this paper; however, it is rather more straightforward to determine their stability to one-dimensional effects. To this end we can examine the time-dependent problem for which we now assume ϕ and ψ are of the form

$$\phi = M_A xy + f(x, t),$$

$$\psi = xy + g(x, t).$$

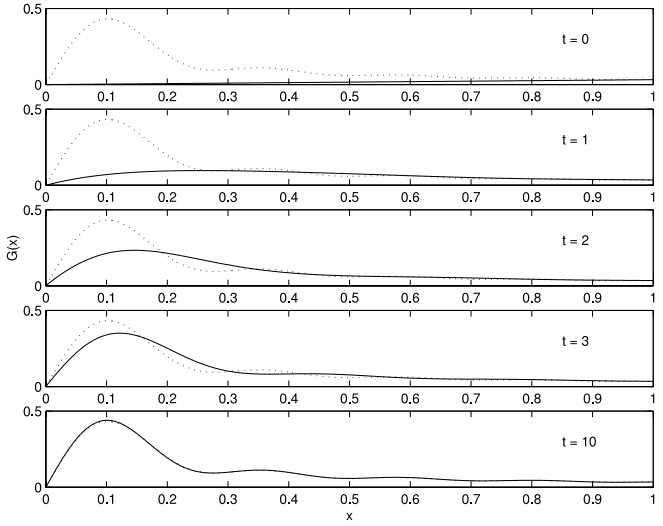

FIG. 4.—Time-dependent evolution of the magnetic shear component $G(x)$ for a Case 2 solution with $A > 0$ and $\nu > 1/2$. The parameter values for this run were $M_A = 2$, $\rho_s = 0.1$, $d_e = 0.04$, and $\eta = 0.0072$, corresponding to $A = 0.0018$, $\gamma = 4$, and $\nu = 3/2$. This sequence of frames shows that an initially linear G profile is swept inward and amplified before settling down into the steady state solution. The steady solution for these parameters, whose analytic form is given by eq. (22), is indicated by the dotted line shown in each frame.

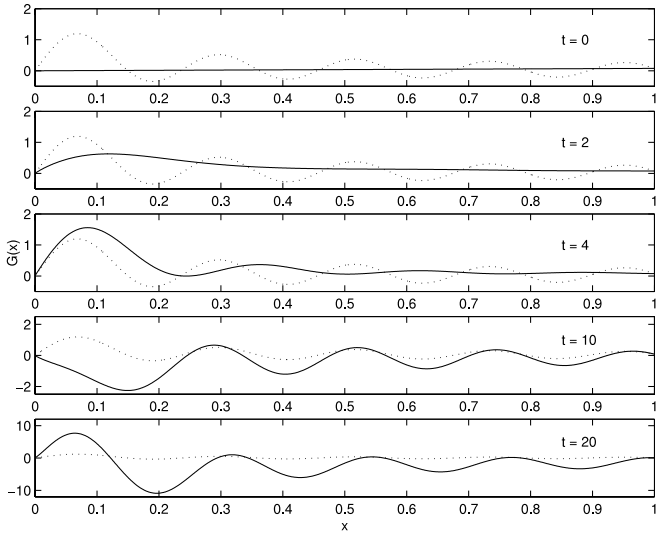

FIG. 5.—Time-dependent evolution of $G(x)$ for a Case 2 solution with $A > 0$ and $\nu < 1/2$. The parameter values for this run were $M_A = 2$, $\rho_s = 0.1$, $d_e = 0.04$, and $\eta = 0.0018$, corresponding to $A = 0.0018$, $\gamma = 1$, and $\nu = 0$. The first few frames show localization and amplification as in Fig. 4; however, once the localization stops and oscillations develop in the outer field, then the wave begins to grow exponentially. The dotted line in each frame once again denotes the (unstable) steady solution. Note the increase in the vertical scale of the last two frames.

We now find that the functions $F = f_x$ and $G = -g_x$ must obey the equations

$$F_t = M_A(xF_x - F) + xG_x - G, \tag{30}$$

$$(G - d_e^2 G_{xx})_t = M_A\left[x(G - d_e^2 G_{xx})\right]_x + [xF_x]_x - \rho_s^2[xF_{xx}]_x + \eta G_{xx} - \eta_2 G_{xxxx}. \tag{31}$$

Note that we have included a hyperresistive term η_2 in the induction equation. This term is needed to regularize the problem at $x = 0$ when $\bar{\gamma} < 1$ as mentioned in § 3. For most simulations it can safely be set to zero, but if it is required it is set at an extremely small value (e.g., $\eta_2 = 10^{-10}$) so that it only acts over a few grid points near the origin and its influence on the rest of the solution is negligible.

Similar time-dependent analyses of the Craig & Henton (1995) problem have been carried out by Craig & Fabling (1998). In addition, a related problem involving one-dimensional electric current and velocity profiles was studied by Bulanov et al. (1990). Their solution, of the form $\phi = B(x, t)$, $\psi = xy + A(x, t)$, showed the rapid decay of the electric current density on a timescale longer than the Alfvén time by a factor of $\ln(4/\eta)$.

In order to test the stability of the steady solutions of § 3, we solve the time-dependent equations over a finite domain. We begin each simulation with an initial configuration in which the functions F and G are given by linear profiles satisfying $F = -\beta G/\alpha$. The values of F and G are then fixed at the boundary as the evolution of the solution proceeds. Note that the initial form of the solution does not influence the final stable equilibrium solution (if one exists). It is only the values of F and G at the boundary that control the final solution; the initial profile only affects the transient phase of the evolution.

For Case 1 solutions with $A = 0$, we find that the initial configuration evolves toward the steady state Dawson function solution for all values of the parameter η.

For Case 2 solutions with $A > 0$, things are more complicated. If resistivity dominates, $\gamma > 2$ and $\nu > 1/2$, then the initial configuration evolves toward the steady state Struve function solution. A typical run in this regime is shown in Figure 4. In this simulation a wave can be seen propagating inward from the outer boundary at $x = 1$. As it approaches the neutral point at $x = 0$ it grows in amplitude, as the flux begins to pileup, and it also begins to develop oscillations in the outer field. The parameters used in this run correspond to $\nu = 3/2$, so the final solution is given by the second formula in equation (22).

If ρ_s dominates with $A > 0$ and $\gamma < 2$ and $\nu < 1/2$, then the one-dimensional steady solutions appear to be unstable, as can be seen in Figure 5. The initial evolution, in which the wave localizes and grows, proceeds as before; however, once the localization stops and oscillations develop in the outer field, the entire wave envelop begins to grow exponentially. The instability of these types of solutions, with their long one-dimensional current sheets, might imply that more general two-dimensional solutions with long, quasi–one-dimensional current sheets are also unstable. This may explain the change in current-sheet topology observed in numerical simulations, from long, thin, quasi–one-dimensional current sheets in resistively dominated plasmas to cross-shaped current structures in collisionless plasmas (Grasso et al. 2001). It is also interesting to note that the change to instability seems to occur at precisely $\nu = 1/2$, and solutions for values of ν less than this have oscillations in the outer field that are so large that there are regions where the magnetic field G changes sign.

For Case 3 when $A < 0$, we find that the steady solution is again stable for all values of μ. An example of this type of solution is shown in Figure 6. Note that when we integrate these solutions we must include a small amount of hyperresistivity to regularize the solution at the origin when $\bar{\gamma} < 1$, as in this regime the second derivatives of F and G are singular at the origin. To check that the hyperresistivity is not having a stabilizing influence, we repeated each simulation at increasing

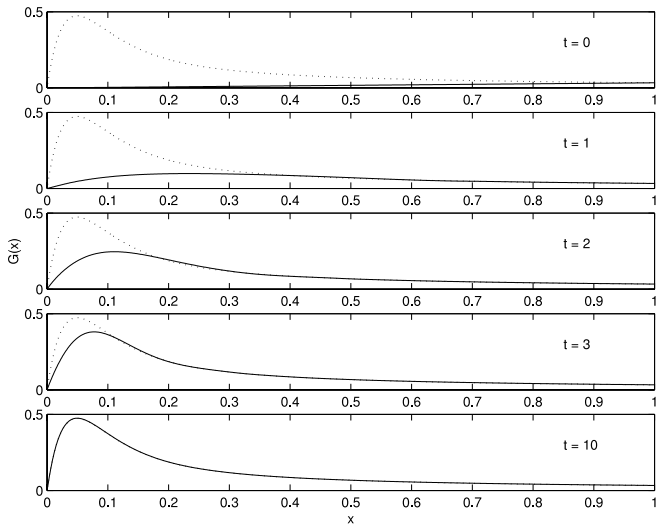

FIG. 6.—Time-dependent evolution of $G(x)$ for a Case 3 solution with $A < 0$. The parameter values for this run were $M_A = 2$, $\rho_s = 0.08$, $d_e = 0.05$, and $\eta = 0.0018$, corresponding to $A = -0.0018$, $\bar{\gamma} = 1$, and $\mu = 1$. Again we see that an initially linear G profile is swept inward and amplified before settling down into the steady state solution denoted by the dotted line.

resolutions, reducing the hyperresistivity each time, in order to limit its effect to a few grid points near the origin. No significant changes in the evolution of the solution or its eventual final equilibrium were observed. The fact that the steady one-dimensional solutions are stable in this regime *might* indicate that quasi–one-dimensional sheets may persist in fully two-dimensional simulations in an electron inertia dominated plasma. Some evidence for this assertion can be found in the simulations of Grasso et al. (2001). These simulations indicate that the cross-shaped structure for the current density and vorticity layers is not as pronounced when $\rho_s \lesssim d_e$, corresponding to $A < 0$ in our notation.

5. CONCLUSIONS

We have derived a family of two-dimensional analytic solutions for the system of equations (4) and (5) that govern weakly collisional plasmas in the strong guide field limit. In this limit the effects of electron compressibility and inertia are more important than the resistivity, and the reconnection process is expected to be significantly modified from that in a collisionally dominated plasma.

Our new solutions are an extension of the Craig & Henton (1995) sheared X-point solutions for a resistive plasma. Despite the new physics involved in the weakly collisional model, the Craig & Henton decomposition of the field and flow still allows us to reduce the complicated two-dimensional partial differential equations to ordinary differential equations that can be solved by elementary techniques. These new types of solution are a departure from usual reconnection models in that they break the fourfold symmetry of the reconnection region that is traditionally imposed. Unlike the more familiar Sweet-Parker and Petschek mechanisms, the reconnection in these types of solution is dominated by highly sheared flows and fields across the reconnection layer. In the symmetric scenario the two field separatrices are on an equal footing, but in the new models they perform different roles. One separatrix (associated with the current sheet) is straight, while the other is highly curved. Mass flow only occurs across the curved field separatrix, but the field is still free to diffuse across the straight separatrix, as this lies in the high-current region where the frozen-in condition of ideal MHD breaks down.

The addition of the collisionless terms into the generalized Ohm's law does not undo the basic behavior of the Craig & Henton–like solutions; however, it does lead to two new solution regimes, depending on the sign of the quantity $A = (\rho_s^2 - M_A^2 d_e^2)/M_A$. If $A > 0$, the plasma behavior is effectively dominated by electron compressibility. The resulting solutions exhibit significant flux pileup and develop large-scale oscillations as the plasma becomes more collisionless. Both these features make the solutions unattractive from a standpoint of achieving fast reconnection. The dramatic flux pileup implies that the solutions would become unphysical in a realistic plasma, and the oscillations rapidly spread out into the surrounding plasma, implying that the process becomes increasingly nonlocal. In fact, in the steady state limit the field oscillations represent a standing kinetic Alfvén wave, which behaves in an identical manner to the standing whistler waves observed in Hall MHD reconnection (Craig & Watson 2003). A further drawback of these solutions is that they appear to become unstable to time-dependent effects when $\nu < 1/2$ and the plasma begins to become collisionless. Indeed, independent two-dimensional simulations (Grasso et al. 2001; Porcelli et al. 2002) show that thin, quasi–one-dimensional current sheets do not persist in this limit and that cross-shaped current features aligned with *both* separatrices develop.

In the other extreme, $A < 0$, the plasma is dominated by electron inertia. The new solutions for this case behave much more like the original Craig & Henton (1995) resistive solutions; however, they have the additional appealing feature that their flux pileup is bounded as the resistivity is decreased. This implies that, for fixed inflow conditions, a fast reconnection rate can be maintained for all values of η. These solutions also appear to be stable, perhaps indicating that the thin one-dimensional sheets so familiar from resistive reconnection simulations may persist in this regime.

Of course the *Ansatz* of a one-dimensional decomposition of the field and flow does not address the stability of these solutions to fully two-dimensional perturbations. Indeed, even in the $A = 0$ and $A < 0$ regimes, in which we might expect long, thin current sheets to persist, the sheets may eventually become unstable to two-dimensional instabilities such as the tearing mode (Biskamp 1986). Behavior such as this could not be explored within the context of our simplified model and would require a full two-dimensional (presumably numerical) treatment.

The authors would like to acknowledge useful discussions with R. Fitzpatrick and I. J. D. Craig.

REFERENCES

Abramowitz, M., & Stegun, I. A. 1972, Handbook of Mathematical Functions (New York: Dover)
Bhattacharjee, A., Ma, Z. W., & Wang, X. 1999, J. Geophys. Res., 104, 14543
Birn, J., et al. 2001, J. Geophys. Res., 106, 3715
Biskamp, D. 1986, Phys. Fluids B, 29, 1520
Biskamp, D. 2000, Magnetic Reconnection in Plasmas (Cambridge: Cambridge Univ. Press)
Bulanov, S. V., Shasharina, S. G., & Pegoraro, F. 1990, Plasma Phys. Controlled Fusion, 32, 377
Craig, I. J. D., & Fabling, R. B. 1996, ApJ, 462, 969

Craig, I. J. D., & Fabling, R. B. 1998, Phys. Plasmas, 5, 635
Craig, I. J. D., Heerikhuisen, J., & Watson, P. G. 2003, Phys. Plasmas, 10, 3120
Craig, I. J. D., & Henton, S. M. 1995, ApJ, 450, 280
Craig, I. J. D., & Watson, P. G. 1999, ApJ, 516, 924
———. 2000, Sol. Phys., 191, 359
———. 2003, Sol. Phys., 214, 131
Grasso, D., Califano, F., Pegoraro, F., & Porcelli, F. 2001, Phys. Rev. Lett., 86, 5051
Hazeltine, R. D., Kotschenreuther, M., & Morrison, P. J. 1985, Phys. Fluids B, 28, 2466
Porcelli, F., Borgogno, D., Califano, F., Grasso, D., Ottaviani, M., & Pegoraro, F. 2002, Plasma Phys. Controlled Fusion, 44, 389
Priest, E. R., & Forbes, T. G. 2000, Magnetic Reconnection: MHD Theory and Applications (Cambridge: Cambridge Univ. Press)
Schep, T. J., Pegoraro, F., & Kuvshinov, B. N. 1994, Phys. Plasmas, 1, 2843
Shay, M. A., Drake, J. F., Rogers, B. N., & Denton, R. E. 2001, J. Geophys. Res., 106, 3759
Vasyliunas, V. M. 1975, Rev. Geophys. Space Phys., 13, 303
Watson, P. G., & Craig, I. J. D. 2002, Sol. Phys., 207, 337